Effect of Finite Domain on von Kármán Profiles Developed in the Neighborhood of Rotating Disk Electrodes

Carlos Domingo Mendez Gaona, carlmendezg@gmail.com

Metallurgy and Materials Engineering Department – Federal University of Rio de Janeiro, PO Box 68505, 1941-972 Rio de Janeiro, RJ, Brazil

Gustavo R. Anjos, gustavo.rabello@gmail.com

Group of Environmental Studies for Water Reservatories – GESAR/State University of Rio de Janeiro, Rua Fonseca Telles 524, 20550-013, Rio de Janeiro, RJ, Brazil

Norberto Mangiavacchi, norberto.mangiavacchi@gmail.com

Group of Environmental Studies for Water Reservatories - GESAR/State University of Rio de Janeiro, Rua Fonseca Telles 524, 20550-013, Rio de Janeiro, RJ, Brazil

José Pontes, jopontes@metalmat.ufrj.br

Metallurgy and Materials Engineering Department – Federal University of Rio de Janeiro, PO Box 68505, 21941-972 Rio de Janeiro, RJ, Brazil

Abstract. *For many years the stability of rotating disk flow has been studied following the evolution of small perturbations superposed to the classical von Kármán's solution, von Kármán (1921, ZAMM, Vol. 19, pp. 233-252), Oliveira (Ms.C dissertation 2011, COPPE/UFRJ). These equations were obtained assuming an infinite domain. In this condition side wall effects are negligible Zandbergen (1987, Fluid Mechanics, Vol. 19, pp. 465-491), Barcia (2000, Journal of The Electrochemical Society, Vol. 155, No. 5, pp. 424-427), Anjos (Ms.C dissertation 2007, COPPE/UFRJ). In the present work we consider the effect of a finite domain on von Kármán's solution, aiming to find the minimum dimensions of the electrochemical cell, bellow which the assumption of von Kármán flow, with nondimensional velocity profiles dependes on the axial coordinate only, no longer holds.*

Keywords: *von Kármán, velocity profiles, Finite Elements Method.*

1. INTRODUCTION

In fluid dynamics, the study of swirling flows is very important due to the large number of applications in different fields. Among them we can cite the fabrication of computer memories by crystal-growth processes, lubrication, aerodynamics, electrochemistry and cosmology Zandbergen P. (1987). This study is usually performed by analysis in the hydrodynamic field of a given domain solving the Navier-Stokes equations. In 1921 von Kámán found a solution of the full hydrodynamic equations describing the flow generated by a large rotating disk.

von Kármán's flow is schematically shown in Fig. (1), with velocity components represented in cylindrical coordinates close to the surface (v_θ, v_r and v_z). Due to the non-slip condition, the flow velocity at the disk surface is equal to the disk velocity at each point of the surface. The rotational movement of the fluid near the surface of the disk has the side effect of inducing by means of centrifugal force, a radial component of the velocity, v_r, which drives the flow away from the axis. The flow must be replaced by an incoming flow approaching disk surface. In addition, experimental setups for rotating disk flows are more easily constructed than setups for more complex geometries. Due to this fact and to the existence of a similarity solution rotating disk flow is widely used as a prototype for studing more complex configurations where cross flow velocity components exist.

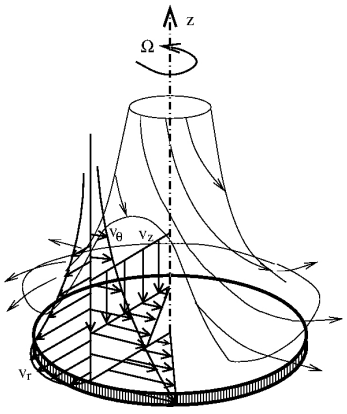

Figure 1. A schematic representation of a rotating disk flow, wich shows the boundary layers relatively to the three velocity components: axial, radial and longitudinal.

Among the several system configurations for which rotating disk flow is a prototype (Barcia (2000), Anjos (2007) and Oliveira (2011)), the solution has been widely adopted in the study of the hydrodynamics of electrochemical cells using rotating disk electrodes.

In particular, the solution has been used for more than 20 years by the group of applied electrochemistry of the Metallurgy and Material Engineering Graduate Program (PEMM/COPPE) to adress phenomena observed in cells using rotating disk electrodes. The experimental setup of electrochemical cells typicaly comprises a rotating disk electrode with diameter about 10 *mm*, which dissolves in the $1MH_2SO_4$ electrolyte solution. For typical angular velocities of the electrode, the thickness of von Kármán's boundary layer is 8-15 times smaller than the electrode diameter. In this condition the flow close to the surface can be approximated by von Kármán's solution.

Barcia (2000) proposed that the dissolution of the iron electrode leads to the existence of a viscosity gradient aligned to the electrode axis, and that this gradient could drive the current instability observed at the beginning of the current *plâteau*. Linear stability analysis performed by Pontes J. (2004) and Mangiavacchi N. (2007) and numerical analysis conduted by Anjos (2007), Oliveira (2011) provide further evidence that the dependency of the electrode viscosity on the concentration of the iron electrode reduces the flow stability indeed.

Given the importance of von Kármán's solution in the study of the hydrodynamics of electrochemical cells it is clear that a knowledge of the effects of the dimensions of the cell on the flow close to the electrode is of paramount importance.

We propose to proceed with previous works of Anjos (2007) and Oliveira (2011), concerning the study of the hydrodynamic field of close to rotating disk, using a finite element approach. These works were developed following the stability analysis performed by Pontes J. (2004) and Mangiavacchi N. (2007), which in turn, were motivated by the work conducted in our group The main idea of the present work consists in finding the influence of a finite domain in the velocity profiles developed in the neighborhood of a rotating disk electrode.

The main goals of this work are as follows: observe the influence of the ratios cell radius/disk radius and cell depth/disk radius on von Kármáns profiles. Specificaly, we are interested in finding how the axial velocity profiles change along the radial direction, in particular, close to electrode surface.

The full Navier-Stokes equations will be solved with a numerical Finite Element code (FEM) featuring a scheme based on Galerkin method for spatial discretization of the diffusive and pressure terms, a scheme based on Semi-Lagrangian method for discretization of the susbtantial derivate ($D\mathbf{v}/Dt$), forward first order representation of time derivatives and a scheme based on the projection method for solving the linear algebraic systems.

The domain is considered fixed and the following boundary conditions are adopted: no-slip condition on the walls $\mathbf{v} = \mathbf{v}(\mathbf{x}, t) = 0$; pressure and velocity in the direction z at the interface electrolyte/air are zero; $p = p(\mathbf{x}, t) = 0$, $\mathbf{v}_z = 0$.

The numerical tests were performed with appropriate selection of domain dimensions and mesh parameters, namely, cell dimensions and mesh refinement, taking into account previous experience of our group.

2. GOVERNING EQUATIONS

The Navier-Stokes and the continuity equations in the nomdimensional form read:

$$\frac{\partial \mathbf{v}}{\partial t} + \mathbf{v} \cdot \nabla \mathbf{v} \;=\; -\frac{1}{\rho}\nabla p + \frac{1}{Re}\nabla \cdot \left[\nu\left(\nabla \mathbf{v} + \nabla \mathbf{v}^T\right)\right] \tag{1}$$

where $\mathbf{v}$, p and ν are the fluid velocity and pressure and kinematic viscosity, respectively. $Re = r(\Omega/\nu)^{1/2}$ is the Reynolds number of the problem, where r is the dimensional radius of the domain and Ω, the angular velocity of the disk. Re is thus, the nondimensional radius of the domain. Further details of variables adimensionalization are given by Anjos (2007).

Boundary and initial conditions

The adoption of proper initial and boundary conditions is essential for the formulation of any problem modeled by PDE's. We apply the following conditions on rigid boundaries;

1. For the initial condition we set the velocity of the fluid to zero in all grid points, except in points located at the disk surface, where we prescribe the angular velocity of the disk, by specifying the corresponding Reynolds number.
2. No-slip condition: viscous flow is defined for the normal component of velocity (v_n) and the tangential components (v_{t1} and v_{t2}) in the solid walls are zero, in obedience to the fact that the fluid immediately adjacent to the wall is in repose in relation to it.
3. Inflow condition: used in boundaries where there is fluid entering the system.
4. Outflow condition: is used where there fronteas system fluid outlet. Once the governig equations are defined, boundary and initial conditions must be prescribed, in order to solve the problem.

3. FINITE ELEMENT METHOD

The fluid flow is given by the equations $\mathbf{v} = \mathbf{v}(\mathbf{x}, t)$ and $p = p(\mathbf{x}, t)$ defined in $\Omega\times$[0,T] when $\Omega \subset \mathbf{R}^m$, so for the the governing equations (1) with $\mathbf{v} = \mathbf{v}_\Gamma$ on Γ_1, $\mathbf{v}_t = 0$ and $\sigma^{nn} = 0$ on Γ_2, where Γ_i, $i = 1, 2, 3$ are respectively the boundary velocity and pressure.

The above expressions are given in nomdimensional form, is important to note that gravity is being depreciated. The space of the test functions is given by $\mathcal{S} := \left\{\mathbf{u} \in \mathcal{H}^1(\Omega) \;\middle|\; \mathbf{u} = \mathbf{u}_c \text{ em } \Gamma_c\right\}$ and the space weighting functions is represented as $\mathcal{V} := \left\{\mathbf{w} \in \mathcal{H}^1(\Omega) \;\middle|\; \mathbf{w} = 0 \text{ em } \Gamma_c\right\}$, where $\mathbf{u}_c$ is an *essential* boundary condition for a given contour Γ_c, $\mathcal{H}^1(\Omega) := \left\{\mathbf{u} \in \mathcal{L}^2(\Omega) \;\middle|\; \frac{\partial \mathbf{u}}{\partial x_i} \in \mathcal{L}^2(\Omega), i = 1, \ldots, n\right\}$, $\mathcal{L}^2(\Omega)$ is the *Lebesgue's space*, which in turn, is the space of square-integrable functions, given by $\mathcal{L}^2(\Omega) := \left\{\mathbf{u} := \Omega \to \mathbf{R}^n \;\middle|\; \left(\int_\Omega |\mathbf{u}|^2 d\Omega\right)^{1/2} < \infty\right\}$.

Expressing the convective term as $\frac{D\mathbf{v}}{Dt} = \frac{\partial \mathbf{v}}{\partial t} + \mathbf{v} \cdot \nabla \mathbf{v}$, the weak formulation for the Navier-Stokes equations can be expressed in the bilinear form:

$$m\left(\frac{D\mathbf{v}}{Dt}, \mathbf{w}\right) - g(p, \mathbf{w}) + \frac{1}{Re} k(\nu; \mathbf{v}, \mathbf{w}) = 0, \tag{2}$$

$$d(q, \mathbf{v}) = 0, \tag{3}$$

Equations (2) and (3) are expressed in matrix form:

$$\mathbf{M}\dot{\mathbf{a}} + \frac{1}{Re}\mathbf{K}\mathbf{a} - \mathbf{G}\mathbf{p} = 0, \tag{4}$$

$$\mathbf{D}\mathbf{a} = 0, \tag{5}$$

where:

$$\mathbf{M} = \begin{bmatrix} \mathbf{M_x} & 0 & 0 \\ 0 & \mathbf{M_y} & 0 \\ 0 & 0 & \mathbf{M_z} \end{bmatrix} \qquad \mathbf{K} = \begin{bmatrix} \mathbf{K_X} & \mathbf{K_{xy}} & \mathbf{K_{xz}} \\ \mathbf{K_{yx}} & \mathbf{K_Y} & \mathbf{K_{yz}} \\ \mathbf{K_{zx}} & \mathbf{K_{zy}} & \mathbf{K_Z} \end{bmatrix}$$

$$\mathbf{K_X} = 2\mathbf{K_{xx}} + \mathbf{K_{yy}} + \mathbf{K_{zz}}, \qquad \mathbf{K_Y} = \mathbf{K_{xx}} + 2\mathbf{K_{yy}} + \mathbf{K_{zz}}, \qquad \mathbf{K_Z} = \mathbf{K_{xx}} + \mathbf{K_{yy}} + 2\mathbf{K_{zz}}$$

$$\mathbf{G} = \begin{bmatrix} \mathbf{G_x} & \mathbf{G_y} & \mathbf{G_z} \end{bmatrix}^T, \qquad \mathbf{D} = \begin{bmatrix} \mathbf{D_x} & \mathbf{D_y} & \mathbf{D_z} \end{bmatrix},$$

$$\dot{\mathbf{a}} = \begin{bmatrix} \dot{\mathbf{u}} & \dot{\mathbf{v}} & \dot{\mathbf{w}} \end{bmatrix}^T, \qquad \mathbf{a} = \begin{bmatrix} \mathbf{u} & \mathbf{v} & \mathbf{w} \end{bmatrix}^T.$$

Semi-Lagrangian method applied to the Navier-Stokes equations

Using the semi-Lagrangian method to the convective term we obtain $\frac{D\mathbf{a}}{Dt} = \frac{\mathbf{a}_i^{n+1} - \mathbf{a}_d^n}{\Delta t}$, thus, Eqs. (2) and (3)are transformed into:

$$m\left(\frac{\mathbf{a}_i^{n+1} - \mathbf{a}_d^n}{\Delta t}, \mathbf{w}\right) - g(p^{n+1}, \mathbf{w}) + \frac{1}{Re} k\left(\nu; \mathbf{a}^{n+1}, \mathbf{w}\right) = 0, \quad (6)$$

$$d(q, \mathbf{a}^{n+1}) = 0, \quad (7)$$

for all $\mathbf{w} \in \mathcal{V}_0$ and $q \in \mathcal{P}_0$, where $\mathrm{a}_d^n = \mathrm{a}^n(x_d, t^n)$, and x_d is called starting point, in time $t^n \leq t \leq t^{n+1}$ with the initial condition $x(t^{n+1}) = x_i$. Therefore the matrix system is:

$$\mathbf{M}\left(\frac{\mathbf{a}_i^{n+1} - \mathbf{a}_d^n}{\Delta t}\right) + \frac{1}{Re}\mathbf{K}\mathbf{a}^{n+1} - \mathbf{G}p^{n+1} = 0 \quad (8)$$

$$\mathbf{D}\mathbf{a}^{n+1} = 0 \quad (9)$$

4. VON KARMAN'S NONDIMENSIONAL VELOCITY PROFILES

Solution of von Kármán's equation for constant viscosity fluids leads to curves of nondimensional profiles *F*, *G* and *H* as shown in Fig 2: The main idea is to solve the full PDE's by Finite Element Method with boundary conditions given in Eq.1 and obtain the local nondimensional profiles *F*, *G* and *H*, according to the formulæ given by Equations 10- 12 at specified radial positions and in different acomplished time steps. The velocity profiles obtained will be compared with von Kármán's original ones.

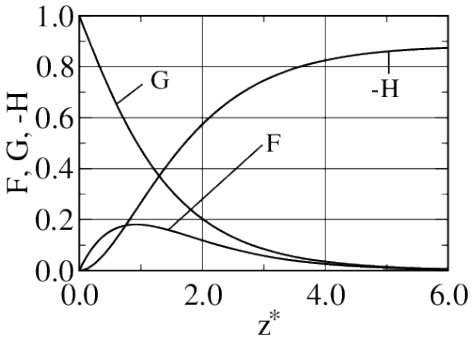

Figure 2. Nondimensional profiles *F*, *G* and *H*, describing the dependence of the velocity components in rotating disk flow.

$$F = \frac{v_r}{r\Omega z^*}, \quad (10)$$

$$G = \frac{v_\theta}{r\Omega z^*}, \quad (11)$$

$$H = \frac{v_z}{(\nu\Omega)^{1/2} z^*}, \quad (12)$$

System configurations

We present the preliminary results of two simulations, which are currently still running. In both, we assume a rotating disk electrode with the lower surface placed at the interface electrolyte/air. The domain radius is equal to the Reynolds number of the simulations. All dimensions are made nondimensional with von Kármán's characteristic legnth, $(\nu/\Omega)^{1/2}$. A scheme of the grid is shown in Fig. 3. The grid consists of a series of regular polygons with center at the z axis, the number of edges of the inner polygon (polygon #1) being specified. The number of edges of the following ones increases by a factor equal to the polygon number. In addition, we specify the number of points along the radial and the axial directions. Points along the radial direction are uniformly spaced. In the axial direction, we adopted a non uniform distribution of points. For the first simulation, the number of edges of the inner polygon, the number of points along the radial direction and the number of points along the axial direction are 6, 20 and 60, respectively. For the second one, the figures are 6, 20 and 57, respectively.

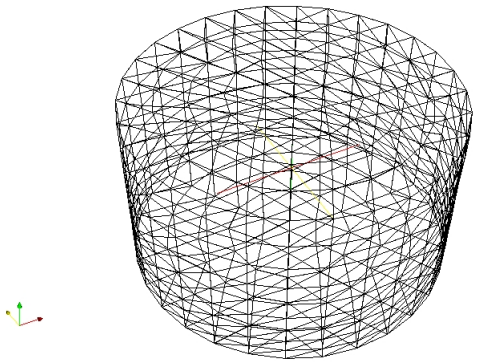

Figure 3. A scheme of the grid used in the two simulations presented in this work.

We monitored the nondimensional velocity profiles, as defined by Eqs. 10, 11 and 12 at three radius denoted r_1, r_2 and r_3 . The domain configuration and dimensions for the two simulations are specified in Fig. 4.

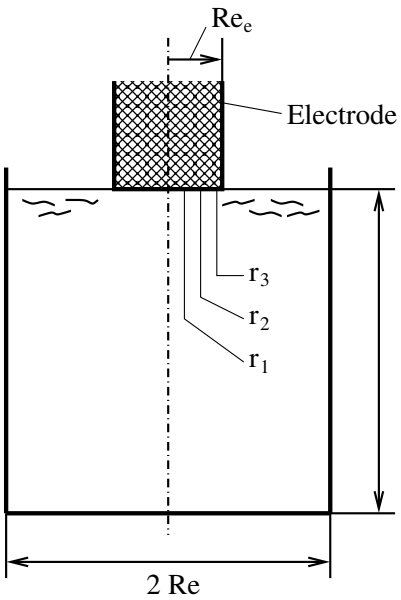

	Simulation 1	Simulation 2
Re	50	300
Re_e	8.33	60
z_{max}	50	650
r_1	2.5	15
r_2	5.0	30
r_3	7.5	45

Figure 4. System configuration and main parameters

5. PRELIMINARY RESULTS

Preliminary results are presented in Figs. 5 and 6. Flow simulations were made with parameters given in Fig. 4. The velocity profiles were converted in the nondimensional profiles F, G and H at three radial positions r_1, r_2 and r_3, in different times and ploted with the steady profiles obtained by numerical integration of von Kármán's system of ODEs. The grid points along the axial position are shown in the profiles obtaned from the FEM simulation.

Both figures contain three columns, each one with von Kármán's original profiles and those obtained at one of the radial positions r_1, r_2 and r_3, but at different times. Higher values of the radial coordinate result in higher local Reynolds numbers and in a progrssive reduction of the stability of the stationary profiles. In consequence, in regions where the stable solution consists of steady state von Kármán's profiles, these profiles are progressively attained from inner to outer radius. This is indeed what we observe in Fig. 5. In this simulation the maximum Reynolds number at the rotating disk is $Re_e = 8.33$, a value that places the whole disk in a region where perturbations are damped and the steady profiles are stable. Clearly, the staedy state is attained first at the inner radius. Of course, the profile H, associated to the axial velocity v_z deviates from von Kármán's profiles for large values of Z, due to the finite domain of the simulation.

Fig. 6 presents the preliminary results of a simulation not yet concluded at the present date, and run at higher Reynolds numbers. In this case, the Reynolds number attained at the disk external radius is $Re_e = 60$, a value for which linear stability analysis point to the existence of undamped perturbations. An inspection of the profiles presented in this figure suggest that the steady state may not be attained at outer radius, or at least, that it will not be attained monotonically.

Proceeding with the present work we intent to adopt a more refined grid close to the disk surface and investigate the effect of different domain radius and depths.

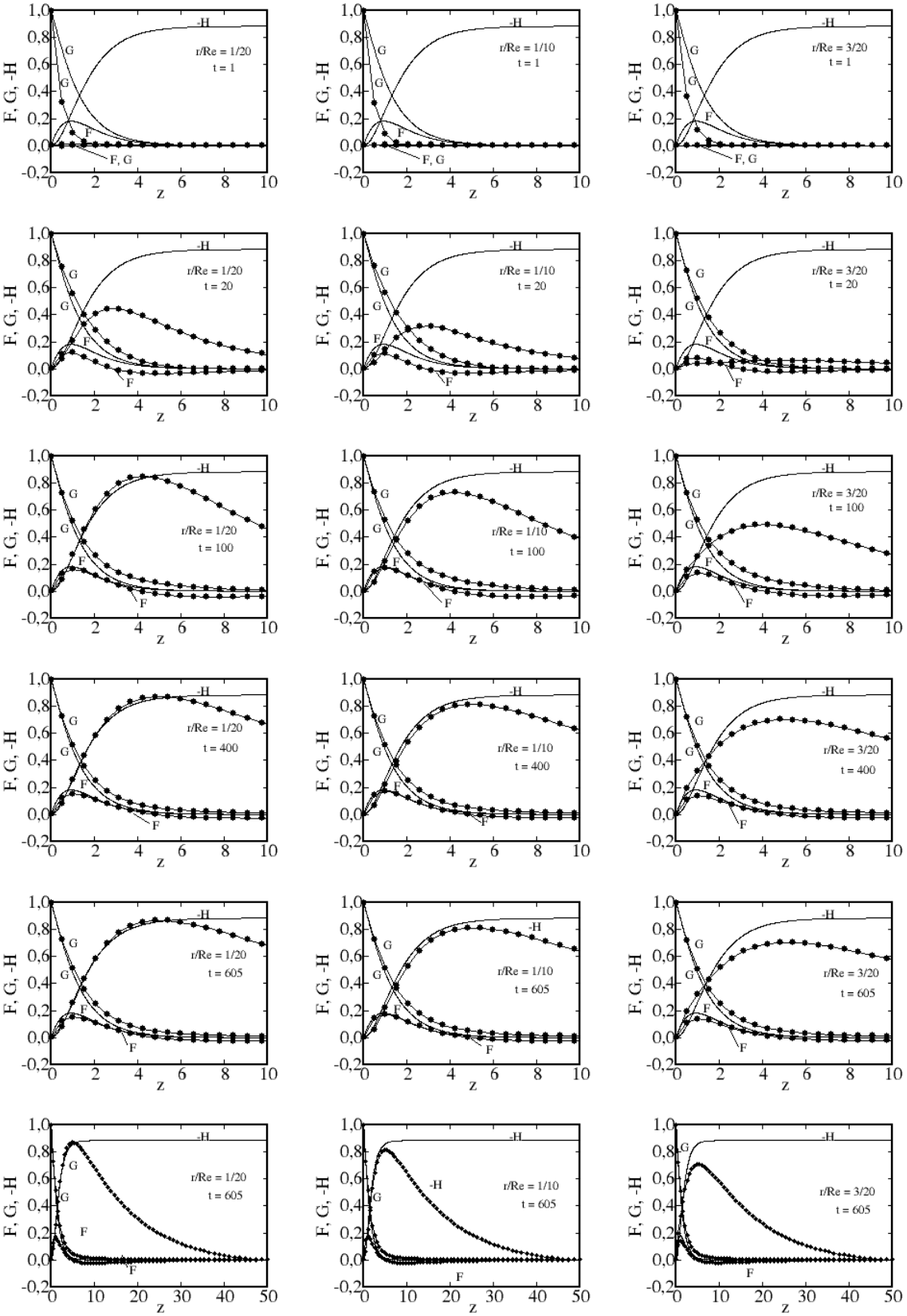

Figure 5. Simulation 1: von Kármán's original profiles F, G and H and same profiles obtained with Eqs. 10, 11 and 12 for a domain and a disk Reynolds number $Re = 50$ and $Re_e = 8.33$, respectively. First column contain profiles at $r_1 = 2.5$; Second column: $r_2 = 5.0$; Third column: $r_3 = 7.5$. Rows 1 to 5 correspond, respectively, to 1, 20, 100, 400 and 605 integration time steps. Row 6 correspond to 605 time steps and showthe $-H$ profile obtained for the entire domain.

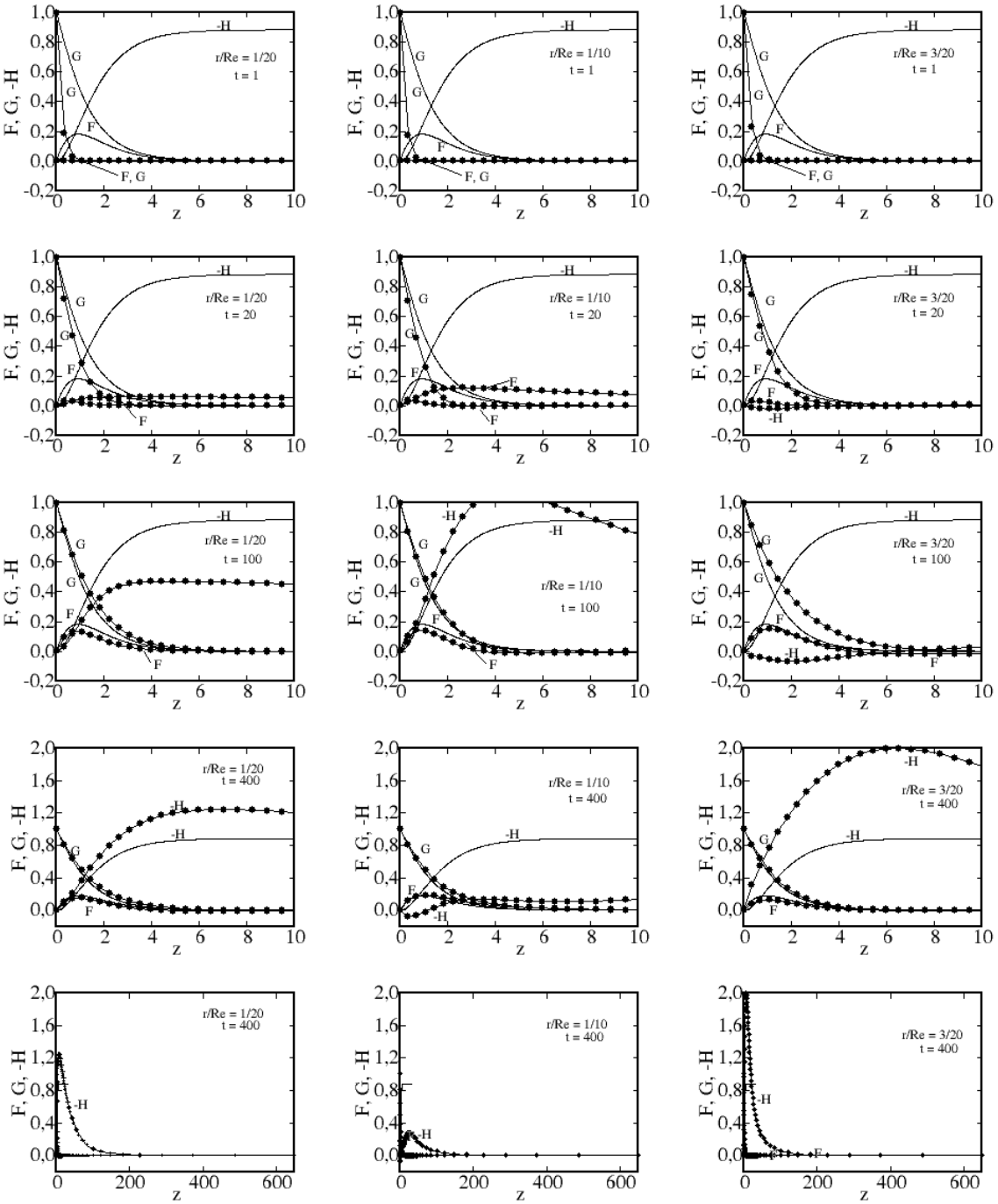

Figure 6. Simulation 2: von Kármán's original profiles F, G and H and same profiles obtained with Eqs. 10, 11 and 12 for a domain and a disk Reynolds number $Re = 300$ and $Re_e = 60$, respectively. First column contain profiles at $r_1 = 15$; Second column: $r_2 = 30$; Third column: $r_3 = 45$. Rows 1 to 4 correspond, respectively, to 1, 20, 100 and 400 integration time steps. Row 5 correspond to 400 time steps and show the $-H$ profile obtained for the entire domain.

6. ACKNOWLEDGMENTS

The authors acknowledge financial support from the Brazilian agencies CAPES and CNPq and the Center for High Performance Computing – NACAD, of the Federal University of Rio de Janeiro, where most simulations here presented were performed. Carlos Mendez also acknowledges financial support from agencies CONACYT (Paraguay).

7. REFERENCES

Anjos, G.R., 2007. *Solução do campo hidrodiâmico em células eletroquímicas pelo Método dos Elementos Finitos*. Ms.C. dissertation, COPPE/UFRJ, Rio de Janeiro, Rio de Janeiro, Brasil.

Barcia, O., 2000. "Rotating disk flow in electrochemical cells: A coupled solution for hydrodynamic and mass equations". *Journal of The Electrochemical Society*, Vol. 155, No. 5, pp. 424–427.

Mangiavacchi N., P.J., 2007. "Rotating-disk flow stability in electrochemical cells: Effect of the transport of a chemical species". *Physics of Fluids*, Vol. 19, pp. 114–119.

Oliveira, G.C.P., 2011. *Estabilidade hidrodinâmica em células eletroquímicas pelo método de elementos finitos*. Ms.C. dissertation, COPPE/UFRJ, Rio de Janeiro, RJ, Brasil.

Pontes J., Mangiavacchi N., C.A.R., 2004. "Rotating-disk flow stability in electrochemical cells: Effect of viscosity stratification". *Physics of Fluids*, Vol. 16, pp. 707–716.

Zandbergen P., D.D., 1987. "von kármán swirling flows". *Fluid Mechanics*, Vol. 19, pp. 465–491.

8. RESPONSIBILITY NOTICE

The following text, properly adapted to the number of authors, must be included in the last section of the paper: The author(s) is (are) the only responsible for the printed material included in this paper.